Izquierdo-Barrientos, M.A.; Sobrino, C.; Almendros-Ibáñez, J.A. (2016) Modeling the heat transfer coefficient between a surface and fixed and fluidized feds with phase change material, In: *Journal of heat transfer (Transactions of the ASME),* 138(7): 072001, 11 pages

DOI: https://doi.org/10.1115/1.4032981

Modeling the heat transfer coefficient between a surface and fixed and fluidized beds with PCM

María A. Izquierdo-Barrientos
ISE Research Group
Thermal and Fluid Eng. Department
Universidad Carlos III de Madrid
Leganés, Spain 28911
Email: maizquie@ing.uc3m.es

C. Sobrino
ISE Research Group
Thermal and Fluid Eng. Department
Universidad Carlos III de Madrid
Leganés, Spain 28911
Email: csobrino@ing.uc3m.es

José A. Almendros-Ibáñez
Escuela de Ingenieros Industriales
Dpto. de Mecánica Aplicada e Ingeniería de Proyectos
Castilla-La Mancha University
Albacete, Spain 02071

Renewable Energy Research Institute
Section of Solar and Energy Efficiency
C/ de la Investigación s/n
Albacete, Spain 02071
Email: jose.almendros@uclm.es

The objective of this work is to model the heat transfer coefficient between an immersed surface and fixed and bubbling fluidized beds of granular phase change material (PCM). The model consists of a two-region model with two different voidages in which steady and transient conduction problems are solved for the fixed and fluidized bed cases, respectively. The model is validated with experimental data obtained under fixed and fluidized conditions for sand, a common material used in fixed and fluidized beds for sensible heat storage, and for a granular PCM with a phase change temperature of approximately 50°C. The superficial gas velocity is varied to quantify its influence on the convective heat transfer coefficient for both materials.

The model proposed for the PCM properly predicts the experimental results, except for high flow rates, which cause the contact times between the surface and particles to be very small and lead the model to over-predict the results.

Nomenclature

A	heat transfer area [m^2]
Ar	Archimedes number [-]
a	submerged area of the probe [m^2]
a_w	parameter that depends on experimental conditions [-]
c_p	specific heat [$J \cdot kg^{-1} \cdot K^{-1}$]

D_t heat transfer probe diameter [m]
d_p particle diameter [m]
H height of the bed [m]
$\overline{h}$ mean heat transfer coefficient [$W \cdot m^{-2} \cdot K^{-1}$]
h_w convective heat transfer coefficient from the bed to the inner surface of the bed [$W \cdot m^{-2} \cdot K^{-1}$]
i enthalpy [J]
k thermal conductivity [$W \cdot m^{-1} \cdot K^{-1}$]
l_s effective length of the solid particles [m]
l_v effective length of the fluid film near the stagnation point of two neighboring particles [m]
m mass [kg]
n number of contact points between two neighboring particles [-]
f_w bubble frequency at the height of the surface [s^{-1}]
Nu Nusselt number [-]
Pr Prandtl number [-]
$\dot{Q}$ heat flux [W]
$\dot{q}$ heat flux per area [$W \cdot m^{-2}$]
q power of the resistance probe [W]
R radius of the particle [m]
R_p particle radius [m]
Re Reynolds number [-]
R equivalent resistance of the heat transferred [$m^3 \cdot K \cdot W^{-1}$]
T temperature [°C]
t time [s]
t time the solids are in contact with the surface [s]
U_{mf} minimum fluidization velocity [$m \cdot s^{-1}$]
$\dot{V}$ flow rate [$m^3 \cdot s^{-1}$]

Greek symbols

α thermal diffusivity [$m^{-2} \cdot s^{-1}$]
β ratio of the distance between the center of two adjacent particles to the particle diameter [m]
ρ density [$kg \cdot m^{-3}$]
σ_{dp} standard deviation of the mean particle diameter [m]
θ angle [rad]
ξ $R \sin\theta$
ε voidage [-]
δ bubble fraction at the wall location [-]
ΔT temperature difference [K]
Δx effective length between the center of two neighboring particles [m]
κ $= k_s/k_g$
ϕ $= l_v/d_p$
γ $= l_s/d_p$
η $= x/(2\sqrt{\alpha t})$

Subscripts

0 ambient/initial
ap apparent
b bed
c contact point
e effective/equivalent
exp experiments
g gas phase
pc phase change
s solid phase
w wall
∞ far from the surface wall

Superscripts

0 motionless fluid

1 Introduction

Extensive research has been conducted evaluating the convective heat transfer coefficient in fixed and fluidized beds [1–8]. In many industrial processes, it is necessary to cool or heat packed or fluidized beds, and this procedure is usually accomplished by the insertion of heat transfer tubes carrying cooling or heating fluids into the bed. The heat transfer occurs between the particle/gas medium and the submerged tube surface (often referred to as the walls). A knowledge of basic mechanisms of heat transfer in beds with immersed heat exchange walls is crucial for producing an optimum design for these systems.

In fluidized beds, the heat transfer coefficient of an immersed surface is several times greater than that for a single-phase gas convection exchanger [9]. Mickley and Fairbanks [10] proposed one of the first models, the so-called “packet theory”, for the heat transfer coefficient between a fluidized bed and a surface. This model treated the heat transfer from surfaces to fluidized beds as the result of the non-steady-state conduction of particle packets at the bed temperature, assuming uniform physical properties. The model successfully explained the role played by the particles in heat transfer processes. However, the model did not account for the non-uniform porosity near the solid wall and predicted infinitely large values of the heat transfer coefficient when

the particle contact time on the heat transfer surface decreased. This model was later improved and developed by considering an additional time-independent resistance near the walls [11, 12]. This additional resistance was treated either as a contact resistance or a gas film with a thickness of $0.1 - 0.33d_p$ by Flamant and Menigault [13]. Kunii and Broughton [4] adopted the packet theory but included a variable property boundary layer to take into account the variation of properties in the packet near the surface due to the porosity variation. Most models required a degree of empiricism to agree with experimental data.

One of the most efficient methods of heat recovery from packed and fluidized beds utilizes horizontally immersed tubes. Information regarding heat transfer to cylinders in a packed bed is sparse when applied to small cylinder sizes (i.e., 1-10 mm). Penny et al. [14] examined heat transfer to cylinders immersed in packed beds in size ranges appropriate for steel wire heat-treating applications and developed an appropriate correlation and an empirical correlation that relates the Nusselt number to relevant physical variables, such as the particle and sample diameters, effective thermal conductivity, and fluid velocity. In another study Penny et al. [15] reported the heat transfer to flat strips immersed in a fluidized bed and the effect of different parameters. Their results are comparable to studies utilizing small cylinders. A number of experimental and numerical investigations have been reported on the measurement of the heat transfer rate between a horizontal tube and fluidized beds [16–25].

The heat transfer coefficient depends on several parameters of the system, such as the size and properties of bed particles, properties of the heat transfer surface (e.g., its geometry, surface finish and orientation within the bed) and the distributor design. Operating parameters, such as temperature, pressure, and fluidizing velocity, also influence the heat transfer process. Di Natale et al. [26] estimated the particle convective heat transfer coefficient in fluidized beds for a broad range of operating conditions and provided a correlation between heat transfer coefficient and surface void fraction. Doherty et al. [19] studied the heat transfer from immersed horizontal tubes of different diameters in gas-fluidized beds. For smooth horizontal tubes, the heat transfer coefficient h_w decreased as the tube diameter increased. This is explained based on the concept that solid particles remain in the vicinity of the heat transfer tube longer as the diameter increases. They found that in all cases, h_w increases with increasing flow rate until a maximum and thereafter slowly decreases. Also they concluded that h_w decreased with increases in the solid particle diameter for the same fluidizing velocity. This trend is in agreement with reported findings in the literature [24, 27–31]. Recent investigations of the heat transfer between horizontally immersed tubes and fluidized beds have focused on larger tubes, i.e., $D_t > 2.5$ cm [32–34]. Few studies have investigated heat transfer from horizontal tubes in the size range of $1 - 8$ mm [35].

Several researchers have evaluated the use of phase-change materials (PCMs) for thermal storage [36–39] due to their ability to store a large amount of energy in a small volume. Trp [40] worked on an experimental and numerical investigation of transient heat transfer phenomena during paraffin melting and solidification in a shell-and-tube latent thermal energy storage unit to provide guidelines for evaluating the system performance and for the design optimization. Experimental and theoretical studies have demonstrated that convection coefficients in fluidized beds are dependent on the energy storage capacity of fluidized particles [41–43]. For this reason, an encapsulated PCM in granular form is expected to enhance the heat transfer rate due to its ability to store large quantities of energy in latent form. Only Brown et al. [44] and Izquierdo-Barrientos et al. [45] measured the heat transfer coefficient in a PCM fluidized bed, however none of them proposed a model to estimate that coefficient. Brown et al. [44] evaluated several types of microencapsulated products as heat transfer media in fluidized beds and observed heat transfer enhancements of 30%. Izquierdo-Barrientos et al. [45] measured the heat transfer between a heated surface immersed in fixed and fluidized beds and granular PCM. They observed that the heat transfer coefficient when there was a phase change in the fluidized PCM

was twice the coefficient when there was no phase change.

In this work, heat transfer coefficients between an immersed horizontal surface and a fixed or fluidized bed with a granular PCM are modeled. The model is also valid for a conventional granular material without PCM. The model of the heat transfer coefficient for a fixed bed is developed according to Yagi and Kunii [46], whereas the model of the heat transfer coefficient for a fluidized bed is developed according to Kunii and Levenspiel [47]. The effective thermal conductivity is a common parameter for both models and is a key parameter in the proper prediction of the heat transfer coefficient. The calculation of this effective thermal conductivity is first attempted. Then, models for heat transfer coefficients in the fixed and fluidized beds are described. Finally, a comparison between the proposed models and experimental results is performed.

2 Model for h_w between a surface and a bed of particles

Schwartz and Smith [48] indicated that the void fraction near the wall surface of a packed bed was larger than in the core of the bed; one particle has only one contact point with the wall surface. Yagi and Kunii [7] concluded that the region of the bed where the voidage is affected by the presence of the wall is extended to a distance of $d_p/2$. Yagi and Kunii [46] and Benenati and Brosilow [49] observed that the voidage in a fixed bed remained constant beyond this distance with a typical value of $\varepsilon_b = 0.4$. Kubie and Broughton [4] proposed a voidage profile near the surface where the voidage varied between 1 at the surface and 0.4 at $x = 0.5\,d_p$. Consequently, it might be reasonable to assume a heat transfer model in which two zones are differentiated by the voidage ε. This model is illustrated in Figure 1.

[Fig. 1 about here.]

In the same manner, the effective thermal conductivity can be separated into two effective thermal conductivity terms: in the bed and in the region adjacent to the surface. Several correlations are proposed in the literature to determine the equivalent conductivity of a packed bed of particles [46, 50–56]. Among these models, equations of the model proposed by Kunii et al. [46,50,51] were chosen. This model is based on the assumption that the total heat transfer through the bed of particles can be divided into two components that flow in parallel

$$\dot{Q} = \dot{Q}_g + \dot{Q}_s, \tag{1}$$

where $\dot{Q}_g$ is the fraction of the heat flux through the gas phase and $\dot{Q}_s$ is the fraction of the heat flux through the solid phase. The radiative heat transfer is neglected for low temperatures.

Figure 2 shows a scheme of the thermal circuit of the heat transfer model where

$$\dot{q}_g = \frac{\dot{Q}_g}{A} = -k_g \varepsilon_b \frac{\partial T}{\partial x} = k_g \varepsilon_b \frac{\Delta T}{\Delta x} \tag{2}$$

and

$$\dot{q}_s = \frac{\dot{Q}_s}{A} = k_s (1-\varepsilon_b) \frac{\Delta T_s}{l_s} = k_g (1-\varepsilon_b) \frac{\Delta T_c}{l_v}. \tag{3}$$

Here, k_s and k_g are thermal conductivities of the solid and gas phases, respectively, and ΔT is the temperature difference for each thermal resistance.

In Figure 2, R_g represents the equivalent resistance of the heat transferred through the gas phase, whereas R_s and R_c represent equivalent resistances for conduction through the solid phase and for conduction through the stagnant fluid near the contact points, respectively.

[Fig. 2 about here.]

The resistances of the thermal circuit are obtained from Equations (2) and (3), yielding

$$R_g = \frac{\Delta x}{k_g \varepsilon_b}, \quad R_s = \frac{l_s}{k_s (1-\varepsilon_b)}, \quad R_c = \frac{l_v}{k_g (1-\varepsilon_b)}, \tag{4}$$

where Δx is the effective length between the center of two neighboring particles in the direction of the heat flow, l_s is the effective length of solid particles and l_v is the effective length of the fluid film near the stagnation point of two neighboring particles [50, 51].

The equivalent resistance of the thermal circuit shown in Figure 2 is

$$R_{eq} = \frac{\Delta x}{k^0_{e,b}} = \left(\frac{1}{R_g} + \frac{1}{R_s + R_c} \right)^{-1}. \tag{5}$$

By introducing different resistances in the previous equation, an expression for the equivalent thermal conductivity of the bed with motionless fluid is obtained

$$\frac{k^0_{e,b}}{k_g} = \varepsilon_b + \frac{\beta_b (1-\varepsilon_b)}{\phi_b + \gamma_b \dfrac{1}{\kappa}}, \tag{6}$$

where $\kappa = k_s/k_g$, $\phi_b = l_v/d_p$, $\gamma_b = l_s/d_p$ and $\beta_b = \Delta x/d_p$ represent ratios of distances between centers of adjacent particles to particle diameters, which, according to Kunii and Smith [50], can be assumed to equal one.

The scheme of two neighboring particles is shown in Figure 3 where the area defined by the radius ξ_0 corresponds to the contact point between the two particles.

[Fig. 3 about here.]

The heat flow through the solid phase is

$$\dot{Q}_s = \int_0^{\xi_0} \mathrm{d}\dot{Q}_s, \tag{7}$$

where

$$\mathrm{d}\dot{Q}_s = 2\pi\xi\,\mathrm{d}\xi \frac{\Delta T}{\dfrac{2R_p\cos\theta}{k_s} + \dfrac{2R_p\,(1-\cos\theta)}{k_g}}. \tag{8}$$

In Equation (8), the area defined by $\mathrm{d}\xi$ is $\mathrm{d}A = 2\pi\xi\,\mathrm{d}\xi$, ΔT is the temperature difference between the center of the two particles and $R_p = d_p/2$ is the particle radius. Taking into account that $\xi = R_b\, sin\theta$, the integration of Equation (8) yields

$$\begin{aligned}\dot{Q}_s =& \pi R_b\, k_g\, \Delta T \left(\frac{\kappa}{\kappa-1} \right)^2 \\ & \left[\ln\left(\kappa - (\kappa-1)\cos\theta_0\right) - \frac{\kappa-1}{\kappa}\left(1-\cos\theta_0\right) \right].\end{aligned} \tag{9}$$

For the thermal model described in Figure 2, the heat flux through the solid phase can also be expressed as

$$\dot{Q}_s = \frac{\pi \left(R_b \sin\theta_0\right)^2 \Delta T}{\dfrac{l_s}{k_s} + \dfrac{l_v}{k_g}}. \tag{10}$$

To solve the system of Equations (9) and (10), where there are 3 unknowns, (l_s, l_v and $\dot{Q}_s$), Kunii and Smith [50] assumed that l_s was the length of a cylinder with the same volume as one particle; therefore, $\gamma = 2/3$ and $l_s = (2/3)d_p$. The expression for ϕ_b is [50]

$$\begin{aligned}\phi_b &= \frac{l_v}{d_p} \\ &= \frac{1}{2}\left(\frac{\kappa-1}{\kappa} \right)^2 \frac{\sin^2\theta_0}{\ln\left(\kappa-(\kappa-1)\cos\theta_0\right) - \dfrac{\kappa-1}{\kappa}\left(1-\cos\theta_0\right)} \\ &\quad - \frac{2}{3}\frac{1}{\kappa}.\end{aligned} \tag{11}$$

Equation (11) is represented in Figure 5(a) as a dashed line. For values of κ less than 10^{-1}, i.e., for thermal conductivities of the particles less than that of the gas, Equation (11) predicts very high values of ϕ_b. Equivalent lengths l_v of hundreds (or even thousands) of factors of the particle diameter are not physically realistic.

Instead of considering the length l_s equal to the length of one cylinder with the same volume of the particle [50], it seems more reasonable to assume that the sum of both lengths, l_s and l_v, is equal to the particle diameter. With this approach, a new model to determine the two lengths l_s and l_v

is presented, where

$$l_v + l_s = d_p \tag{12}$$

and thus,

$$\phi_b + \gamma_b = 1. \tag{13}$$

Under these statements and following a similar line of reasoning as Kunii and Smith [50], a new expression for ϕ_b is obtained

$$\begin{aligned}\phi_b &= \frac{l_v}{d_p} \\ &= \frac{1}{2}\left(\frac{\kappa-1}{\kappa}\right)\frac{\sin^2\theta_0}{\ln\left(\kappa-(\kappa-1)\cos\theta_0\right)-\dfrac{\kappa-1}{\kappa}\left(1-\cos\theta_0\right)} \\ &\quad -\frac{1}{\kappa-1}.\end{aligned} \tag{14}$$

This expression is plotted in Figure 5(b). In this case, the value of ϕ_b is less than one, i.e., $l_v < d_p$, for any value of κ.

To obtain the required ϕ_b, the angle θ_0 must be determined. This angle is related to the number of contact points n between two neighboring particles and follows the expression [50]

$$\sin^2\theta_0 = \frac{1}{n}. \tag{15}$$

To estimate n, two particle arrangements should be considered: one for the most open packing and one for close packing [50]. It was assumed that actual packed beds with particle size distributions may be composites of both packing states. Thus, the correct value for ϕ_b is an additive function between ϕ_1 and ϕ_2

$$\phi_b = \phi_2 + (\phi_1 - \phi_2)\frac{\varepsilon_b - \varepsilon_2}{\varepsilon_1 - \varepsilon_2}, \tag{16}$$

where ϕ_1 is obtained for the less packed bed with $n_1 = 1.5$; $\varepsilon_1 = 1-\pi/6$ and ϕ_2 are obtained for the close packed bed with $n_2 = 4\sqrt{3}$; and $\varepsilon_2 = 1-\sqrt{2}\pi/6$.

To obtain the equivalent thermal conductivity in the region adjacent to the heat transfer surface, a similar line of reasoning as that used for Equation (6) is followed, which yields

$$\frac{k^0_{e,w}}{k_g} = \varepsilon_w + \frac{\beta_w(1-\varepsilon_w)}{\phi_w + \gamma_w\dfrac{1}{\kappa}}, \tag{17}$$

where the subscript w indicates that all variables are evaluated in the region adjacent to the wall surface. As stated in Yagi and Kunii [46], the region of the bed where the voidage is affected by the presence of the wall is extended to a distance of $d_p/2$. As a consequence, for a thickness of $d_p/2$, $\beta_w = 1/2$.

The heat flux through the particles near the wall surface can be calculated following a similar line of reasoning. When the particles touch the surface, it is assumed that the angle θ_0, which defines the region of contact, is equal to $\pi/2$, i.e., $\xi_0 = d_p/2$, and extends to a region of length $d_p/2$ (see Figure 4).

[Fig. 4 about here.]

Given these premises, then

$$\begin{aligned}\dot{Q}_s &= \int_0^{\xi_0} 2\pi\xi\, d\xi \frac{\Delta T}{\dfrac{R_p\cos\theta}{k_s}+\dfrac{R_p\,(1-\cos\theta)}{k_g}} \\ &= \pi d_p k_g \Delta T\left(\frac{\kappa}{\kappa-1}\right)^2\left[\ln\kappa-\frac{\kappa-1}{\kappa}\right].\end{aligned} \tag{18}$$

The heat flux can also be expressed as

$$\dot{Q}_s = \frac{\frac{\pi}{4} d_p^2 \Delta T}{\frac{l_{s,w}}{k_s} + \frac{l_{v,w}}{k_g}}, \tag{19}$$

where $l_{s,w}$ and $l_{v,w}$ are the effective length of solid particles and the fluid film at the wall surface, respectively.

Combining Equations (18) and (19), the expression of ϕ_w is

$$\phi_w = \frac{l_{v,w}}{d_p} = \frac{1}{4}\left(\frac{\kappa-1}{\kappa}\right)^2 \frac{1}{\ln\kappa - \frac{\kappa-1}{\kappa}} - \frac{1}{3}\frac{1}{\kappa}. \tag{20}$$

Figure 5(a) shows the variation of ϕ_w with κ according to the previous equation. For values of κ less than 10^{-1}, Equation (20) results in negative values, which are physically unrealistic.

As before, an alternative model for determining the two lengths $l_{s,w}$ and $l_{v,w}$ is applied

$$l_{s,w} + l_{v,w} = \Delta x_w = d_p/2, \tag{21}$$

and thus,

$$\gamma_w + \phi_w = \beta_w = 1/2. \tag{22}$$

Equation (21) indicates that the lengths of the two branches of the thermal circuit shown in Figure 2 are equal to half of one diameter, which is the distance from the surface where a different voidage is assumed.

Thus, the expression of ϕ_w is

$$\phi_w = \frac{l_{v,w}}{d_p} = \frac{1}{4}\left(\frac{\kappa-1}{\kappa}\right) \frac{1}{\ln\kappa - \frac{\kappa-1}{\kappa}} - \frac{1}{2(\kappa-1)}. \tag{23}$$

Figure 5 shows variations of ϕ_b and ϕ_w with κ for the two models. The original equations proposed by Yagi and Kunii [46,51], with $\gamma_b = 2/3$ and $\gamma_{b,w} = 1/3$, predict values greater than one or negative for $\phi_{b,w}$, which is physically unrealistic. For the model, we propose that these values are less than one, i.e., l_v and $l_{v,w}$ are less than the particle diameter.

[Fig. 5 about here.]

2.1 Fixed Bed

As stated by Yagi and Kunii [7], the convective heat transfer coefficient between a wall surface and a packed bed h_w can be expressed as

$$\frac{h_w d_p}{k_g} = \frac{h_w^0 d_p}{k_g} + a_w Re\, Pr, \tag{24}$$

where k_g is the thermal conductivity of the gas, h_w^0 is the wall film coefficient with a motionless fluid and Re and Pr are the Reynolds and Prandtl numbers, respectively. The parameter a_w depends on flow conditions, the Reynolds number and particle sizes; its value varies, depending on the material and experimental conditions.

It is assumed that particles in contact with the wall surface are surrounded by stagnant, motionless fluid [46].

According to Yagi and Kunii [46], the heat transfer coefficient between a surface and a packed bed with a stagnant fluid h_w^0 can be obtained

$$-k_{e,w}^0 \left.\frac{\partial T}{\partial x}\right|_{x=0} = -k_{e,b}^0 \left.\frac{\partial T}{\partial x}\right|_b = h_w^0 (T_w - T_{ap}), \tag{25}$$

where $k_{e,w}^0$ and $k_{e,b}^0$ are the aforementioned equivalent thermal conductivities (i.e., Equations (6) and (17), respectively), T_w is the wall temperature, T_{ap} is the extrapolation of the temperature profile within the bed to $x = 0$ (i.e., the apparent temperature), $\partial T/\partial x|_{x=0}$ represents the temperature slope in the region close to the surface ($x < d_p/2$) and $\partial T/\partial x|_b$ represents the variation of the temperature in the bed, far from the influence of the heat transfer surface.

From Figure 1, partial derivatives of Equation (25) can be computed as follows

$$k^0_{e,w}\,\frac{T_w - T_b}{d_p/2} = k^0_{e,b}\,\frac{T_{ap} - T_b}{d_p/2} = h^0_w\,(T_w - T_{ap})\,. \tag{26}$$

Solving the system, the expression obtained is

$$\frac{2}{\dfrac{d_p\,h^0_w}{k_g}} = \frac{1}{\dfrac{k^0_{e,w}}{k_g}} + \frac{1}{\dfrac{k^0_{e,b}}{k_g}}. \tag{27}$$

Equation (27) calculates h^0_w if the equivalent thermal conductivity in the bed $k^0_{e,b}$ and the equivalent thermal conductivity near the wall surface $k^0_{e,w}$ are known. The model can be used whether the granular material contains PCM or not.

2.2 Fluidized Bed

The classical concepts of two phases (i.e., emulsion and bubble) and packet renewal ([10]) are used in this model because the model is considered a bubbling gas-solid fluidized bed [57]). In this way, the average heat transfer coefficient between an immersed surface and fluidized particles can be expressed as [58]

$$h_w = \delta\,\bar{h}_g + (1-\delta)\,\bar{h}_s, \tag{28}$$

where δ is the bubble fraction at the wall location and $\bar{h}_g$ and $\bar{h}_s$ account for the convection for the period when the surface is bathed by bubbles and for the period when the surface is bathed by emulsion packets, respectively. Radiation contributions are neglected due to low temperatures.

The convective component $\bar{h}_g$ can be obtained from Baskakov et al. [59]

$$\bar{h}_g = 0.009\,\frac{k_g}{d_p}\,Ar^{0.5}\,Pr^{0.33}, \tag{29}$$

where Ar is the Archimedes number. This correlation has been accepted by many researchers as a good estimation of the gas convective coefficient over a wide range of fluidizing conditions [24, 60–65]. The contribution from the gas phase will be low due to the lower thermal conductivity of the gas phase compared to the dense phase.

When a group of particles touches a heated surface, a transient heat transfer occurs between the surface at T_s and the group of particles that are initially at the temperature of the bed T_b. The group of particles, following the model of heat transfer through packed beds presented earlier, can be studied as a two-region model. One region has a thickness $d_p/2$ and a voidage ε_w adjacent to the surface; a second region exists at a distance larger than $d_p/2$ from the surface and has a voidage ε_b. Therefore, to determine the heat transferred from the surface to the dense phase, a one-dimensional conduction problem through two regions with different properties has to be solved (see dashed-profiles in Figure 1). The equation to solve is

$$\frac{\partial T}{\partial t} = \alpha\frac{\partial^2 T}{\partial x^2}, \tag{30}$$

where T is the temperature and α is the equivalent thermal diffusivity, which is equal to

$$\alpha_{x\le d_p/2} = \frac{k^0_{e,w}}{(\rho\,c_p)_w}, \tag{31}$$

$$\alpha_{x>d_p/2} = \frac{k^0_{e,b}}{(\rho\,c_p)_b}. \tag{32}$$

Variables with the subscript w are evaluated with ε_w, and variables with the subscript b are evaluated with ε_b. Under typical fluidization conditions with air, the volumetric heat capacities of solids are several orders of magnitude larger than that of air, such that their expressions can be approximated as

$$(\rho c_p)_w \approx (1-\varepsilon_w)\,(\rho c_p)_s, \tag{33}$$

$$(\rho c_p)_b \approx (1-\varepsilon_b)\,(\rho c_p)_s. \tag{34}$$

To solve Equation (30), it is convenient to introduce a change of variable

$$\eta = \frac{x}{2\sqrt{\alpha t}}, \tag{35}$$

which transforms the partial differential equation (30) into an ordinary differential equation

$$\frac{\mathrm{d}^2 T}{\mathrm{d}\eta^2} = -2\eta\frac{\mathrm{d}T}{\mathrm{d}\eta}. \tag{36}$$

The solution of this equation is in the form [66]

$$T_{x\leq d_p/2} = C_1\,\frac{\sqrt{\pi}}{2}\,\mathrm{erf}\,(\eta_w) + C_2, \tag{37}$$

$$T_{x>d_p/2} = C_3\,\frac{\sqrt{\pi}}{2}\,\mathrm{erf}\,(\eta_b) + C_4, \tag{38}$$

where η_w and η_b are variables defined in Equation (35) evaluated near and far from the surface, respectively. Boundary conditions necessary to obtain constants $C_{i=1..4}$ and their values are presented in Appendix A.

The instantaneous heat transfer coefficient on the surface when the solids are in contact can be determined as

$$-k_w\,\left.\frac{\partial T}{\partial x}\right|_{x=0} = h_s\,(T_w - T_\infty)\,. \tag{39}$$

By introducing the derivative of the temperature profile in the above Equation (37), an expression for the instantaneous heat transfer coefficient is obtained

$$h_s = \frac{-A\,k_w}{\sqrt{\pi\alpha_w t}\left[\mathrm{erf}\left(\eta_{b_{x=d_p/2}}\right) - \mathrm{erf}\left(\eta_{w_{x=d_p/2}}\right)A - 1\right]}, \tag{40}$$

where erf is the error function and

$$A = \frac{k_b}{k_w}\sqrt{\frac{\alpha_w}{\alpha_b}}\exp\left(\mathrm{erf}\left(\eta_{b_{x=d_p/2}}\right) - \mathrm{erf}\left(\eta_{w_{x=d_p/2}}\right)\right) \tag{41}$$

is a function that varies with time. The average heat transfer coefficient during the time t_s that solids are in contact with the surface is expressed as

$$\bar{h}_s = \frac{1}{t_s}\int_0^{t_s} h_s(t)\,\mathrm{d}t, \tag{42}$$

which has to be computed numerically. The time t_s can be estimated as

$$t_s = \frac{1-\delta}{f_w}, \tag{43}$$

where f_w is the bubble frequency at the height of the surface. Small variations in the contact times strongly affect mean values of the heat transfer coefficient. Most correlations found in the literature for the contact time of a packet with a surface refer to vertical walls. The bubbling frequency inside the bed is larger than that in a vertical wall, so the time t_s is smaller. For our experimental conditions, we have observed that the evolution of the packed residence time with the superficial gas velocity follows the correlation proposed by Lu et al. [5], proposed for vertical walls, with an approximate difference of 0.1 s. So, we have calculated t_s by the correlation of Lu et al. [5] minus 0.1 s.

The numerical integration of Equation (42) is not easy to compute because h_s approaches infinity as the time approaches zero. An alternative approach to compute $\bar{h}_s$ is to define the instantaneous Nusselt number

$$Nu_s = \frac{h_s\sqrt{\pi\alpha_w t}}{k_w}, \tag{44}$$

where $\sqrt{\pi\alpha_w t}$ is the characteristic length of the problem.

Hence, the average Nusselt number is

$$\overline{Nu}_s = \frac{\bar{h}_s \sqrt{\pi \alpha_w t_s}}{k_w}. \tag{45}$$

From Equation (42), the average Nusselt number can be expressed as

$$\overline{Nu}_s = \frac{1}{t_s} \int_0^{t_s} \frac{\sqrt{\pi \alpha_w t_s}}{k_w} h_s(t)\, \mathrm{d}t. \tag{46}$$

Introducing the change of variable

$$\beta = \sqrt{\pi \alpha_w t}, \tag{47}$$

the average Nusselt number can be computed as

$$\overline{Nu}_s = \frac{2}{\beta_s} \int_0^{\beta_s} Nu_s(t)\, \mathrm{d}\beta, \tag{48}$$

where the integral

$$\int_0^{\sqrt{\pi \alpha_w t_s}} Nu_s(t)\, \mathrm{d}\beta = \\ = \int_0^{\sqrt{\pi \alpha_w t_s}} \frac{-A}{\left[\mathrm{erf}\left(\eta_{b_{x=d_p/2}}\right) - \mathrm{erf}\left(\eta_{w_{x=d_p/2}}\right) A - 1\right]} \mathrm{d}\beta \tag{49}$$

is easier to compute numerically as Nu_s approaches one and $\overline{Nu}_s$ approaches two as time approaches zero. Once the average Nusselt number is obtained, the average heat transfer coefficient $\bar{h}_s$ can be obtained from Equation (45).

Figure 6(a) shows the instantaneous and mean heat transfer coefficients calculated using the theoretical model for the sand as a function of the flow rate. Figure 6(b) presents corresponding contact times for the same flow rates. The higher the flow rate, the greater the heat transfer coefficient and the quicker the contact time.

[Fig. 6 about here.]

2.3 Fluidized bed with granular material with PCM

If the solid phase is filled with a PCM, the governing equation of the heat transfer process is

$$\frac{\partial i_s}{\partial t} = \frac{k}{\rho} \frac{\partial^2 T}{\partial x^2}, \tag{50}$$

where $k = k^0_{e,w}$ and $\rho = \rho_w$ if $x \leq d_p/2$, $k = k^0_{e,b}$ and $\rho = \rho_b$ if $x > d_p/2$ and i_s is the enthalpy of the PCM (represented graphically in Figure 8), which is a non-linear function of temperature during the phase change process, as it is explained later in Section 3. This equation has an analytical solution if the phase change process occurs at constant temperature. Solutions for different geometries can be found in [67]. If the phase change takes place over a range of temperatures, the equation should be solved numerically. Indeed, because the phase change occurs over a temperature range, the equation is numerically solved using an explicit finite difference scheme. A uniform spatial step of $\Delta x = 25$ μm and a time step of $\Delta t = 6.5 \cdot 10^{-5}$ s are used. Once the non-steady-state problem is solved, the heat transfer coefficient can be computed according to Equation (39), and the mean value over the time t_s can be found by Equation (42).

The heat transfer coefficients obtained through the model for the PCM as a function of the flow are depicted in Figure 7(a), and corresponding contact times for each flow are also shown in Figure 7(b).

[Fig. 7 about here.]

3 Comparison of the model with experimental results

The experiments carried out by Izquierdo-Barrientos et al. [45] for the commercial PCM GR50 Rubitherm and the sand are used to validate the proposed model. The PCM is available in two particle sizes. A coarser size is used in the

fixed bed because its minimum fluidization is above the 1000 l/min flow rate; a finer size is used in the fluidized bed. Table 1 presents several properties of the sand and PCM, such as the density ρ, thermal conductivity k, mean diameter of the particles $\overline{d}_p$ with its standard deviation σ_{dp} and the approximate mass m used for each experiment.

The enthalpy evolution with temperature for the PCM GR50 is presented in Figure 8. The data shown in this figure is obtained by differential scanning calorimetry (DSC) with a slow heating rate of 0.5°C/min [36,68]. The phase change of the PCM is distinguished at approximately 50°C, which is its phase change temperature T_{pc}. These data are used to evaluate Equation (50). Thus, for each time step, values for i_s are calculated, and then the temperature is determined from the calculated enthalpy using the function presented in Figure 8.

[Table 1 about here.]

[Fig. 8 about here.]

The experimental apparatus used for the heating experiments is the same used by Izquierdo-Barrientos et al. [45], which consists of a cylindrical tube with an internal diameter of 200 mm filled with particles. The air flow that enters the column can be heated by electrical heaters. Type K thermocouples are placed along the axis to measure the bed temperature at different heights, T_∞. In the same locations, the heat transfer probe can be introduced, which consists of a cylindrical variable resistance of 200 W with three thermocouples distributed around its surface. This probe is similar to the one used by Masoumifard et al. [24]. The three thermocouples permit the measurement of the mean temperature of the resistance surface, T_w.

The bed temperature is uniform and equal to the ambient temperature $T_0 \simeq 18$°C at the beginning of every experiment. The air is introduced into the column at the desired rate and once the bed reaches steady state, the heat transfer probe is heated to a temperature higher than the phase change temperature of the PCM T_{pc}. For these conditions, the temperatures at different heights of the bed and the probe temperature are measured over a 1-min period at a frequency of 1 Hz.

The experimental heat transfer coefficient is calculated following the expression

$$h_w = \frac{q}{a(T_w - T_\infty)}, \tag{51}$$

where a is the submerged area of the probe and q is the heat rate transferred by the probe. The heat rate supplied to the probe is varied during the experiments to obtain a temperature difference of $T_w - T_\infty \approx 20$°C, where $T_\infty \approx 35$°C.

3.1 Fixed bed

Figure 9 displays the experimental results from Izquierdo-Barrientos et al. [45] and the model results for the sand and the PCM in the packed bed. The experimental data for the heat transfer coefficient are plotted in the form of the Nusselt number, $Nu = (h_w \cdot d_p)/k_g$, as a function of the product between the Reynolds and Prandtl numbers, using Equation (24). The slope of the linear regression corresponds to the parameter a_w. For $a_w = 0.29$ for the sand and $a_w = 0.25$ for the PCM, the model reasonably predicts the value of Nusselt number and therefore, the heat transfer coefficient. The stagnant fluid model result for the Nusselt number, $Nu^0 = (h_w^0 \cdot d_p)/k_g$, obtained by Equation (27), yields 4.18 for the PCM and 4.20 for the sand, which agrees with the experimental results (see Figure 9). The wall surface used in experiments by Izquierdo-Barrientos et al. [45] is a small-diameter cylindrical wall. A larger voidage at the wall is expected due to the curved profile of the probe and the small ratio between the probe and particle diameter, D_t/d_p. Therefore, the voidage affected by the presence of the wall is $\varepsilon_w = 0.9$.

[Fig. 9 about here.]

3.2 Fluidized bed

Figure 10(a) shows the total heat transfer coefficients obtained for the sand from the experiments by Izquierdo-Barrientos et al. [45] and from the model of a fluidized bed. The minimum fluidization velocity of the sand, U_{mf}, is 0.33

m/s, which corresponds to 622 l/min. Therefore, all selected flow rates are above this value [45]. As observed for the fixed bed case, the heat transfer coefficient increases when the flow rate increases. The proposed model (continuous line) predicts trends similar to the results observed in the experiments, with approximately constant differences. These differences can be attributed to uncertainties in the value of the equivalent thermal conductivity [4]. Kubie and Broughton [4] observed similar differences in their experimental data. Figure 10(a) shows that a reduction of 20% of the equivalent thermal conductivity at the wall results in decreased heat transfer coefficient, getting a better agreement with the experiments. There are various parameters that influence on the final value of the equivalent thermal conductivity, such as: the solid conductivity of the material, the voidage, the grade of packing of the particles, etc.

Figure 10(b) displays the total heat transfer coefficients obtained from the experiments and from the model for the PCM. In the case of the PCM, the minimum fluidization velocity is $U_{mf} = 0.13$ m/s, which corresponds to a flow rate of 250 l/min [45]. The selected flow rates for the PCM experiments are above 250 l/min. The model is observed to fit the experimental data for nearly all selected flow rates. At higher flow rates, the model does over-predict the transfer coefficients. Additionally, at these higher rates, the smaller contact times do not allow the PCM to complete its phase change. For instance, for a flow rate of 500 l/min, the contact time for the granular PCM is approximately 0.1 s (see Figure 7(b)). The corresponding characteristic length for this contact times is $\sqrt{\pi \alpha_w t} \simeq d_p/2$ which means that the heat conduction do not penetrate the whole particle, thus, the granulate does not completely melt.

[Fig. 10 about here.]

4 Conclusions

The proposed model for the heat transfer coefficient in packed beds was validated with experiments carried out with sand and a PCM. The potential benefit of the phase change of PCM is limited because there is no renovation of the particles touching the heat transfer surface, which are the ones where the PCM is in liquid form.

The model of the heat transfer coefficient in a fluidized bed properly predicts the trend of h_w when the sand and the PCM are fluidized. Only for very short contact times between the PCM and the wall surface does the model over-predict heat transfer coefficients. Small deviations of the model prediction for the sand may be due to uncertainties in parameters introduced in the model, such as the equivalent thermal conductivity [4].

Acknowledgements

This work was partially funded by the Spanish Government (Project ENE2010-15403), the regional Government of Castilla-La Mancha (Project PPIC10-0055-4054) and Castilla-La Mancha University (Project GE20101662).

References

[1] Botterill, J., and Desai, M., 1972. "Limiting factor in gas-fluidized bed heat transfer". *Powder Technol.,* **6**, pp. 231–238.

[2] Chen, J., 1976. "Heat transfer to tubes in fluidized bed". In National Heat Transfer Conference, no. 76-HT-75.

[3] Mickley, H., and Trilling, C., 1949. "Heat transfer characteristics of fluidized beds". *Ind. Eng. Chem.,* **41**, pp. 1135–1147.

[4] Kubie, J., and Broughton, J., 1975. "A model of heat transfer in gas fluidized beds". *Int. J. Heat Mass Tran.,* **18**(2), pp. 289 – 299.

[5] Lu, J., Flamant, G., and Snabre, P., 1993. "Towards a general model for vertical wall to gas-solid fluidized beds heat transfer. i particle convection and gas convection". *Chem. Eng. Sci.,* **48**, pp. 2479–2492.

[6] Zhang, R., H. Yang, J. L., and Wu, Y., 2013. "Theoretical and experimental analysis of bed-to-wall heat trans-

fer in heat recovery processing". *Powder Technol.,* **249**, pp. 186–195.

[7] Yagi, S., and Kunii, D., 1960. "System on heat transfer near wall surface in packed beds". *A. I. Ch. E. J.,* **6**, pp. 97–104.

[8] Kunii, D., and Suzuki, M., 1966. "Heat transfer between wall surface and packed solids". In International Heat Transfer Conference IV, A. I. Ch. E., pp. 344–352.

[9] Chen, J., 2003. *Handbook of fluidization and fluid-particle systems*. Taylor & Francis Group LLC, ch. Heat Transfer.

[10] Mickley, H., and Fairbanks, D., 1955. "Mechanism of heat transfer to fluidized beds". *A. I. Ch. E. J.,* **1**, pp. 374–384.

[11] Baskakov, A., 1964. "The mechanism of heat transfer between a fluidized bed and a surface". *Int. J. Chem. Eng,* **4**, pp. 320–324.

[12] Patel, R., 1967. Surface-renewal model for heat transfer between wall and fluidized beds. ANL-7353 110, Research and Development Report.

[13] Flamant, G., and Menigault, 1987. "Combined wall-to-fluidized bed heat transfer. Bubble and emulsion contributions at high temperature". *Int. J. Heat Mass Tran.,* **30**, pp. 1803–1812.

[14] Penny, C., Naylor, D., and Friedman, J., 2010. "Heat transfer to small cylinders immersed in a packed bed". *Int. J. Heat Mass Tran.,* **53**, pp. 5183–5189.

[15] Penny, C., Rosero, D., Naylor, D., and Friedman, J., 2011. "Heat transfer to flat strips immersed in a fluidized bed". *ASME J. Heat Transfer,* **133**, p. 71703.

[16] Wood, R., Staub, F., Canada, G., and McLaughlin, M., 1978. Two-phase flow and heat transfer. Tech. Rep. 525-1, General Electric Co.

[17] Vreedenberg, H., 1958. "Heat transfer between a fluidized bed and a horizontal tube". *Chem. Eng. Sci.,* **1**, pp. 52–60.

[18] Chandran, R., Chen, J., and Staub, F., 1980. "Local heat transfer coefficient around horizontal tubes in fluidized beds". *A. I. Ch. E. J.,* **102**(152-157).

[19] Doherty, J., Verma, R., Shrivastava, S., and Saxena, S., 1986. "Heat transfer from immersed horizontal tubes of different diameter in a gas fluidized bed". *Energy,* **11**, pp. 773–783.

[20] Grewal, N., and Saxena, S., 1979. "Effect of surface roughness on heat transfer from horizontal immersed tubes in fludized bed". *Transactions of American Institute of Mechanical Engineers Journal Heat Transfer,* **101**, pp. 397–403.

[21] Lese, H., and Kermode, R., 1972. "Heat transfer from a horizontal tube to a fluidized bed in the presence of unheated tubes". *Can. J. Chem. Eng.,* **50**, pp. 44–48.

[22] Bartel, W., and Genetti, W., 1973. "Heat transfer from a horizontal bundle of bare and finned tubes in an air fluidized bed". *Chemical Engineering Progress Symposium Series,* **69**, pp. 85–93.

[23] Priebe, S., and Genetti, W., 1977. "Heat transfer from a horizontal bundle of extended surface tubes to an air fluidized bed". *Chemical Engineering Progress Symposium Series,* **73**, pp. 38–43.

[24] Masoumifard, N., Mostoufi, N., Hamidi, A.-A., and Sotudeh-Gharebagh, R., 2008. "Investigation of heat transfer between a horizontal tube and gas-solid fluidized bed". *International Journal of Heat and Fluid Flow,* **29**, pp. 1504–1511.

[25] Natale, F. D., Bareschino, P., and Nigro, R., 2010. "Heat transfer and void fraction profiles around a horizontal cylinder immersed in a bubbling fluidised bed". *Int. J. Heat Mass,* **53**, pp. 3525–3532.

[26] Natale, F. D., Lancia, A., and Nigro, R., 2008. "A single particle model for surface-to-bed heat transfer in fluidized beds". *Powder Technol.,* **187**, pp. 68–78.

[27] Grewal, N., and Saxena, S., 1980. "Heat transfer between a horizontal tube and a gas-solid fluidized bed". *Int. J. Heat Mass Tran.,* **23**, pp. 1505–1519.

[28] Grewal, N., and Saxena, S., 1977. "Investigation of heat transfer from immersed tubes in a fluidized bed". In Fourth National Heat Mass Transfer Conference, pp. 53–58.

[29] Grewal, N., Saxena, S., Dolidovich, A., and Zabrodsky, S., 1979. "Effect of distributor design on heat transfer from an immersed horizontal tube in a fluidized bed". *Chem. Eng. J.,* **18**, pp. 197–201.

[30] Botterill, J., 1975. *Fluid-Bed Heat Transer*. Academic Press, New York.

[31] Kim, S., Ahn, J., Kim, S., and Lee, D., 2003. "Heat transfer and bubble characteristics in a fludized bed with immersed horizontal tube bundle". *Int. J. Heat Mass Tran.,* **399-409**.

[32] Khan, T., and Turton, R., 1992. "The measurements of instantaneous heat transfer coefficients around the circumference of a tube immersed in a high temperature fluidized bed". *Int. J. Heat Mass Tran.,* **35**, pp. 3397–3406.

[33] Karamavruc, A., and Clark, N., 1996. "A correction factor for one-dimensional heat transfer coefficients around a horizontal tube in a fluidized bed". *Powder Technol.,* **86**, pp. 209–217.

[34] Li, H., Qian, R., Huang, W., and Bi, K., 1993. "An investigation on instantaneous local heat transfer coefficients in high temperature fluidized beds. i experimental results". *Int. J. Heat Mass Tran.,* **36**, pp. 4389–4395.

[35] Friedman, J., and D. Naylor, P. K., and Rosero, D., 2006. "Heat transfer to small horizontal cylinders immersed in a fluidized bed". *Transactions of the ASME, Journal Heat Transfer,* **128**, pp. 984–988.

[36] Rady, M., 2009. "Granular phase change materials for thermal energy storage: experiments and numerical simulations". *Appl. Therm. Eng.,* **29**, pp. 3149–3159.

[37] Regin, A., Solanki, S., and Saini, J., 2009. "An analysis of a packed bed latent heat thermal energy storage system using PCM capsules: Numerical investigation". *Renew. Energ.,* **34**, pp. 1765–1773.

[38] Nallusamy, N., Sampath, S., and Velarj, R., 2006. "Study on performance of a packed bed latent heat thermal energy storage unit integrated with solar water heating system". *Journal of Zhejiang University SCIENCE A,* **8**, pp. 1422–1430.

[39] Izquierdo-Barrientos, M.A., Sobrino, C., and Almendros-Ibáñez, J.A., 2013. "Thermal energy storage in a fluidized bed of PCM". *Chem. Eng. J.,* **230**(0), pp. 573 – 583.

[40] Trp, A., 2005. "An experimental and numerical investigation of heat transfer during technical grade paraffin melting and solidification in a shell-and-tube latent thermal energy storage unit". *Sol. Energy,* **79**(6), pp. 648 – 660. Polymeric Materials for Solar Energy Applications.

[41] Ziegler, E., Koppel, L., and Brazelton, W., 1964. "Effects of solid thermal properties on heat transfer to gas fluidized beds". *Industrial & Engineering Chemistry Fundamentals,* **3**, pp. 324–328.

[42] Molerus, O., 1992. "Heat transfer in gas fluidized beds. part i". *Powder Technol.,* **70**, pp. 1–14.

[43] Brown, R., and Overmann, S., 1998. "The influence of particle thermal time constants on convection coefficients in bubbling fluidized beds". *Powder Technol.,* **98**, pp. 13–20.

[44] Brown, R., Rasberry, J., and Overmann, S., 1998. "Microencapsulated phase-change materials as heat transfer media in gas fluidized beds". *Powder Technol.,* **98**, pp. 217–222.

[45] Izquierdo-Barrientos, M. A., Sobrino, C., and Almendros-Ibáñez, J. A., 2015. "Experimental heat transfer coefficient in fixed and fluidized beds with PCM". *Appl. Therm. Eng.,* **78**, pp. 373–379.

[46] Yagi, S., and Kunii, D., 1962. "Studies on heat transfer in packed beds". *Int. Dev. Heat Tran.*, pp. 750–759.

[47] Kunii, D., and Levenspiel, O., 1991. *Fluidization Engineering*. Butterworth-Heinemann, Stoneham, USA.

[48] Schwartz, C., and Smith, J., 1953. *Industrial and Engineering Chemistry*. pp. 45–1209.

[49] Benenati, R., and Brosilow, C., 1962. "Void fraction distribution in beds of spheres". *A. I. Ch. E. J.,* **8**, pp. 359–361.

[50] Kunii, D., and Smith, J., 1960. "Heat transfer characteristics of porous rocks". *A. I. Ch. E. J.,* **6**, pp. 71–78.

[51] Yagi, S., and Kunii, D., 1957. "Studies on effective thermal conductivities in packed beds". *A. I. Ch. E. J.,* **3**, pp. 373–381.

[52] Krupiezka, R., 1967. "Analysis of thermal conductivity in granular materials". *Int. J. Chem. Eng,* **7**, pp. 122–144.

[53] Vortmeyer, D., and Adam, W., 1984. "Steady-state measurements and analytical ccorrelation of axial effective thermal conductivities in packed beds at low flo rates.". *Int. J. Heat Mass Tran.,* **27**, pp. 1465–1472.

[54] Elsari, M., and Hughes, R., 2002. "Axial effective thermal conductivities of packed beds". *Appl. Therm. Eng.,* **22**, pp. 1969–1980.

[55] Gonzo, E., 2002. "Estimating correlation for the effective thermal conductivity of granular materials". *Chem. Eng. J.,* **90**, pp. 299–302.

[56] Wen, D., and Ding, Y., 2006. "Heat transfer of gas flow through a packed bed". *Chem. Eng. Sci.,* **61**, pp. 3532–3542.

[57] Geldart, D., 1973. "Types of gas fluidization". *Powder Technol.,* **7**, pp. 285–292.

[58] Grace, J., Leckner, B., Zhu, J., and Cheng, Y., 2006. *Mutiphase Flow Handbook*. Taylor & Francis, ch. Fluidized beds, pp. 1–93.

[59] Baskakov, A., Berg, B., Vitt, O., Filippovsky, N., Hirakosyan, V., Goldobin, J., and Maskaev, V., 1973. "Heat transfer to objects immersed in fluidized beds". *Powder Technol.,* **8**, pp. 273–282.

[60] Glicksman, L., and Decker, N., 1980. "Design relationships for predicting heat transfer to tube bundles in fluidized bed combustion". In Proceedings of the Sixth Annual International Conference on Fluidized Bed Combustors, Vol. III, p. 152.

[61] Modrak, T., 1979. Fluidized bed combustion development facility and commercial utility afbc design assessment. Tech. rep., Quarterly technical progress report prepared for ERPI.

[62] Groenewold, H., and Tsotsas, E., 2007. "Drying in fluidized beds with immersed heating elements". *Chem. Eng. Sci.,* **62**, pp. 481–502. Fluidized Bed Applications.

[63] Natale, F. D., Lancia, A., and Nigro, R., 2009. "Surface-to-bed heat transfer in fluidised beds of fine particles". *Powder Technol.,* **195**, pp. 135–142.

[64] Merzsch, M., Lechner, S., and Krautz, H. J., 2013. "Heat-transfer from single horizontal tubes in fluidized beds: Influence of tube diameter, moisture and diameter-definition by Geldart C fines content". *Powder Technol.,* **235**, pp. 1038–1046.

[65] Kim, S. W., and Kim, S. D., 2013. "Heat transfer characteristics in a pressurized fluidized bed of fine particles with immersed horizontal tube bundle". *Int. J. Heat Mass Tran.,* **64**, pp. 269–277.

[66] Nellis, G., and Klein, S., 2009. *Heat Transfer*. Cambridge University Press.

[67] Mehling, H., and Cabeza, L. F., 2008. *Heat and cold storage with PCM*. Springer, Berlin, Germany.

[68] Rady, M., 2009. "Study of phase changing characteristics of granular composites using differential scanning calorimetry". *Energ. Convers. Manage.,* **50**, pp. 1210–1217.

Appendix A

In this appendix, the boundary conditions necessary to obtain constants $C_{i=1...4}$ in Equations (37) and (38) are explained. The boundary conditions consist of a fixed temperature at the wall surface and continuity in the temperature and its first derivative at the interface between both mediums. Additionally, at locations far away from the heat transfer surface, the temperature of the solid phase should be equal to the initial temperature. In this manner, the boundary conditions are:

boundary condition at $x = 0$

$$T|_{x=0} = T_w \tag{52}$$

first boundary condition at $x = d_p/2$

$$T|_{x=d_p/2^-} = T|_{x=d_p/2^+} \tag{53}$$

second boundary condition at $x = d_p/2$

$$\dot{q}_{x=d_p/2} = -k_w \left.\frac{\partial T}{\partial x}\right|_{x=d_p/2^-} = -k_b \left.\frac{\partial T}{\partial x}\right|_{x=d_p/2^+} \quad (54)$$

boundary condition at $x \to \infty$

$$\lim_{x\to\infty} T = T_\infty. \quad (55)$$

Introducing these boundary conditions into Equations (37) and (38), and after some manipulation, the constants are:

$$C_1 = \frac{2}{\sqrt{\pi}} A \frac{T_w - T_\infty}{\operatorname{erf}\left(\eta_{mf_{x=d_p/2}}\right) - \operatorname{erf}\left(\eta_{w_{x=d_p/2}}\right) A - 1} \quad (56)$$

$$C_2 = T_w \quad (57)$$

$$C_3 = \frac{2}{\sqrt{\pi}} \frac{T_w - T_\infty}{\operatorname{erf}\left(\eta_{mf_{x=d_p/2}}\right) - \operatorname{erf}\left(\eta_{w_{x=d_p/2}}\right) A - 1} \quad (58)$$

$$C_4 = T_\infty - \frac{T_w - T_\infty}{\operatorname{erf}\left(\eta_{mf_{x=d_p/2}}\right) - \operatorname{erf}\left(\eta_{w_{x=d_p/2}}\right) A - 1}. \quad (59)$$

List of Figures

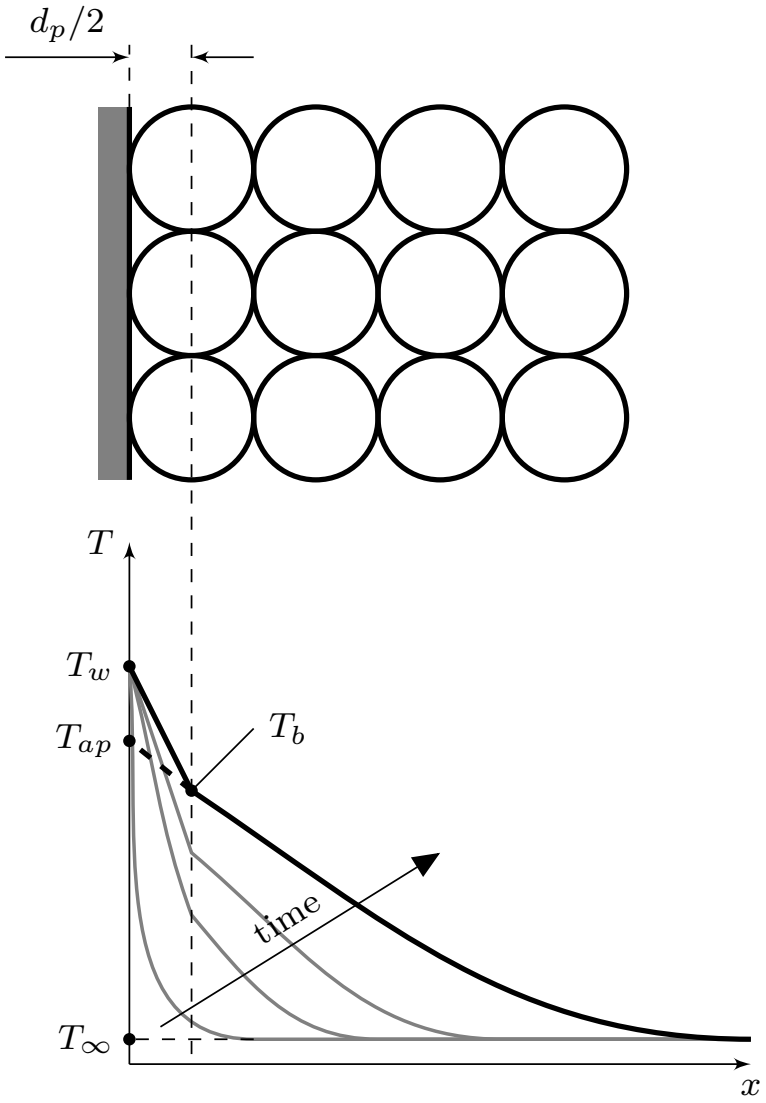

Fig. 1. Temperature profile in a packed bed in the region near the wall, where T_w is the wall/surface temperature, T_b is the bed temperature at a distance $d_p/2$ from the surface, T_∞ is the bed temperature far from the wall and T_{ap} is the extrapolation of the temperature profile within the bed to $x = 0$ (apparent temperature)

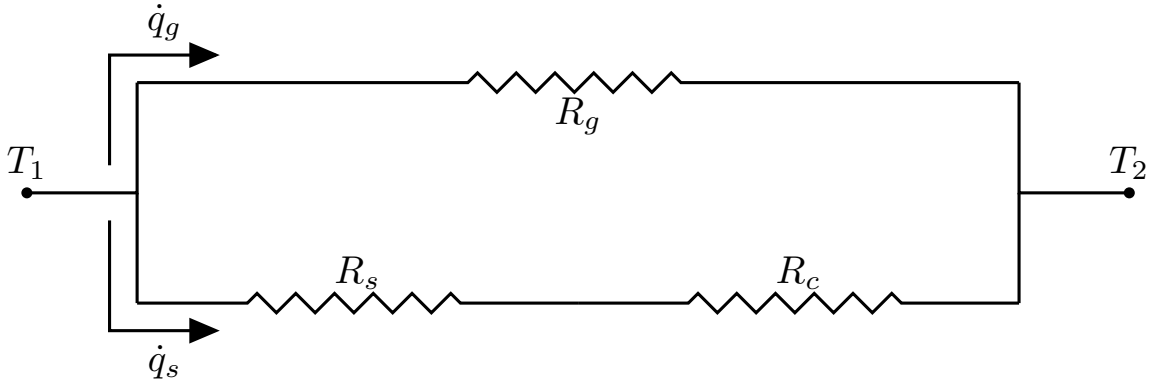

Fig. 2. Equivalent thermal circuit of the heat transfer model through a bed of particles

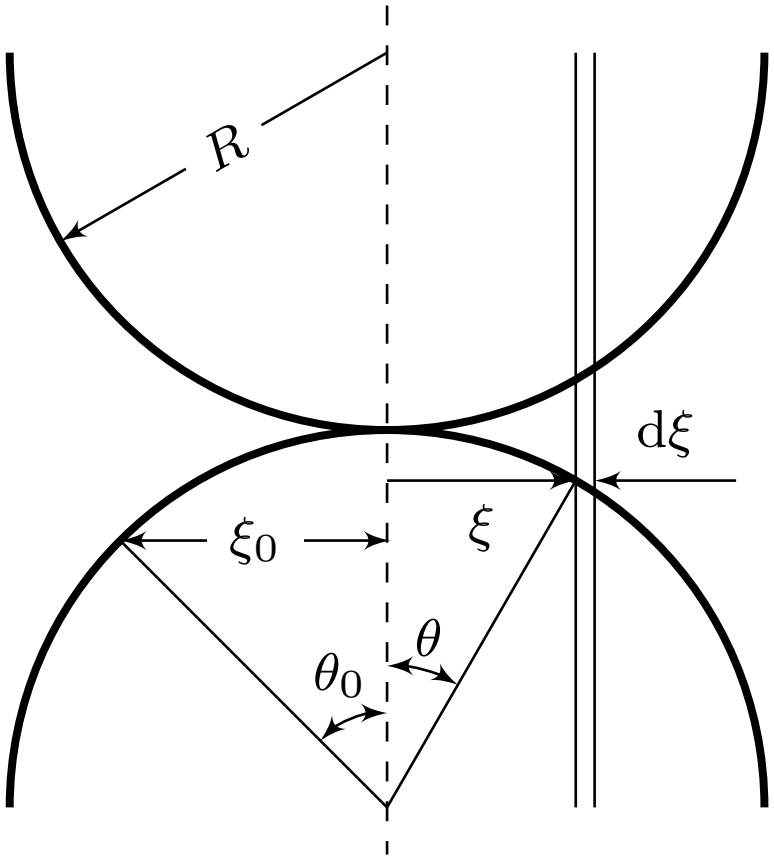

Fig. 3. Scheme of two neighboring particles for determining $\dot{Q}_s$

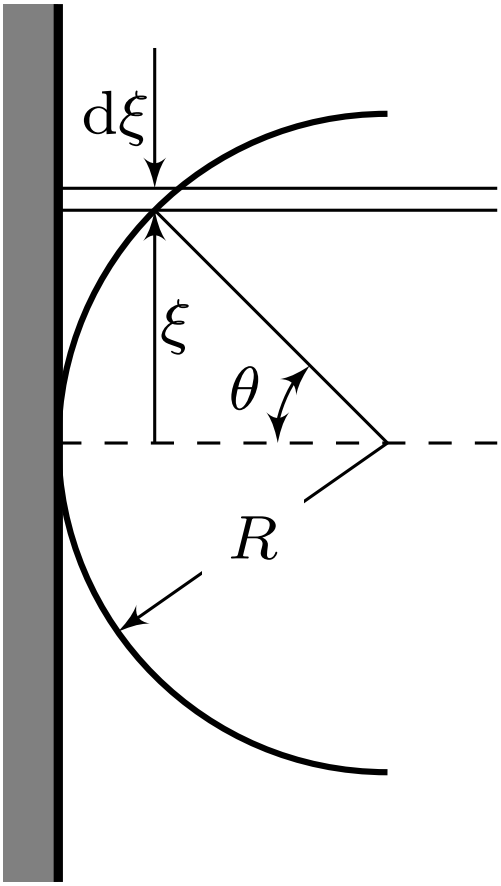

Fig. 4. Scheme for determining $\dot{Q}_s$ at the wall surface

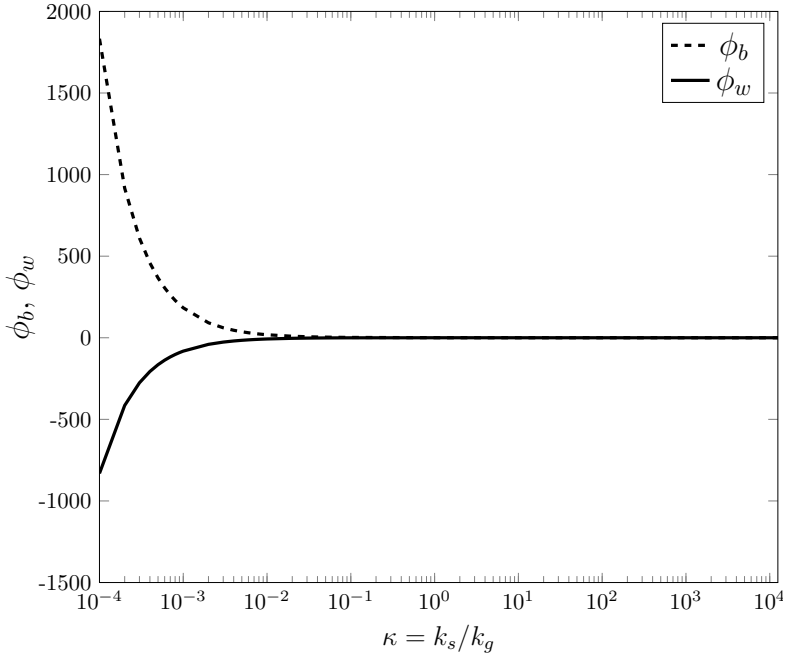

(a) Kunii and Smith [50]

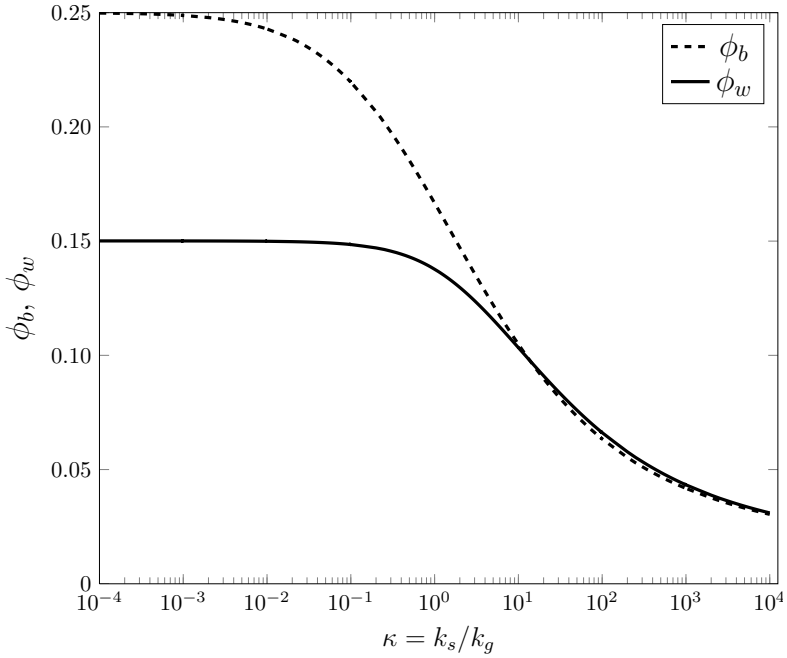

(b) Proposed model

Fig. 5. Graphical representation of ϕ_b and ϕ_w for two models and different values of κ. The data for ϕ_b are calculated for $\varepsilon_b = 0.4$

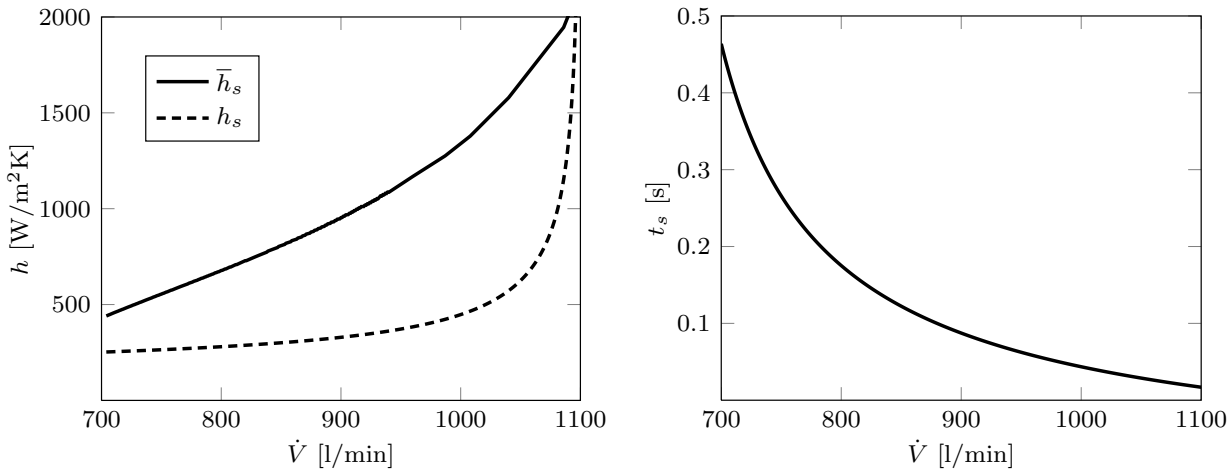

(a) (b)

Fig. 6. (a) Evolution of the mean $\overline{h}_s$ and instantaneous h_s heat transfer coefficient for the sand as a function of the flow rate. (b) Corresponding contact times for the flow rate

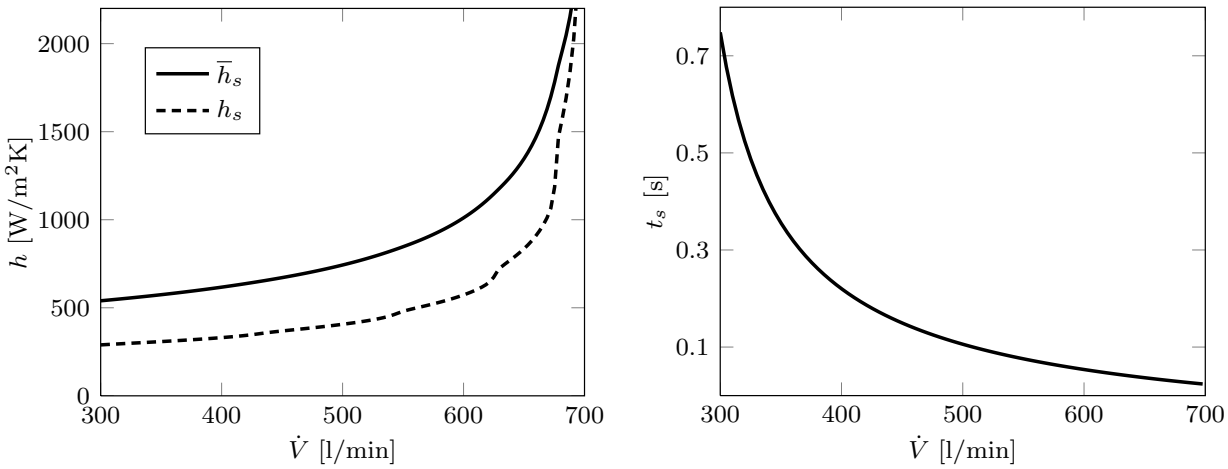

(a) (b)

Fig. 7. (a) Evolution of the mean $\overline{h}_s$ and instantaneous h_s heat transfer coefficient for the PCM as a function of the flow rate. (b) Corresponding contact times for the flow rate

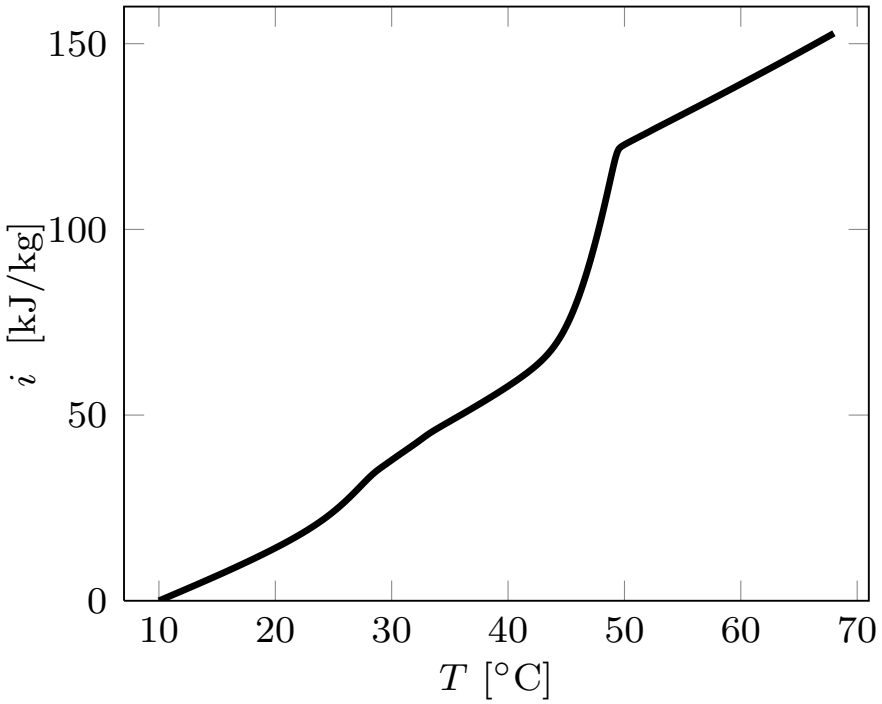

Fig. 8. Enthalpy variation with temperature for the PCM GR50.

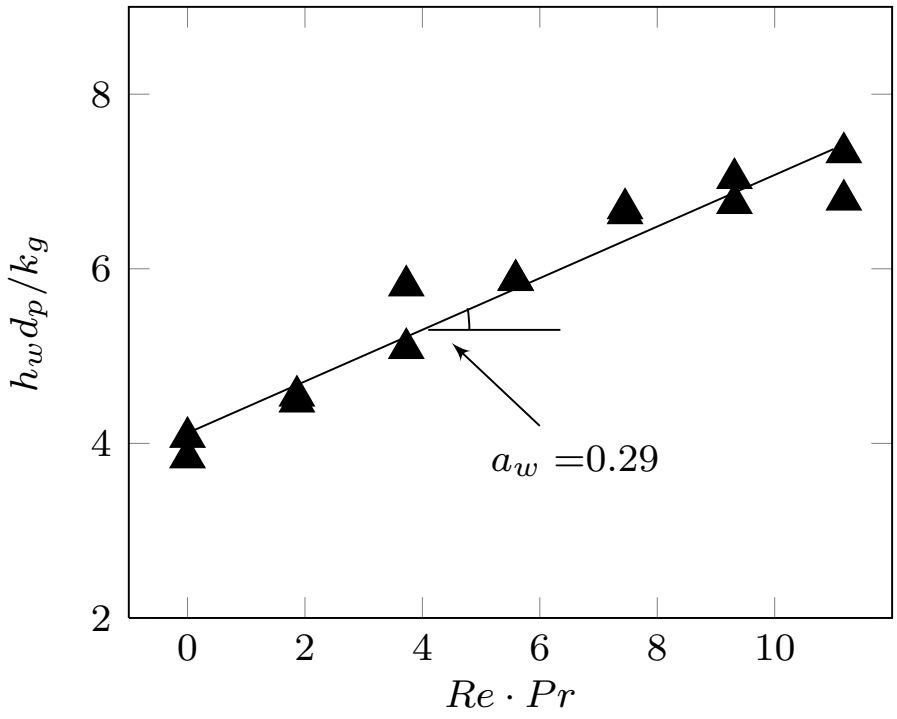

(a) Sand

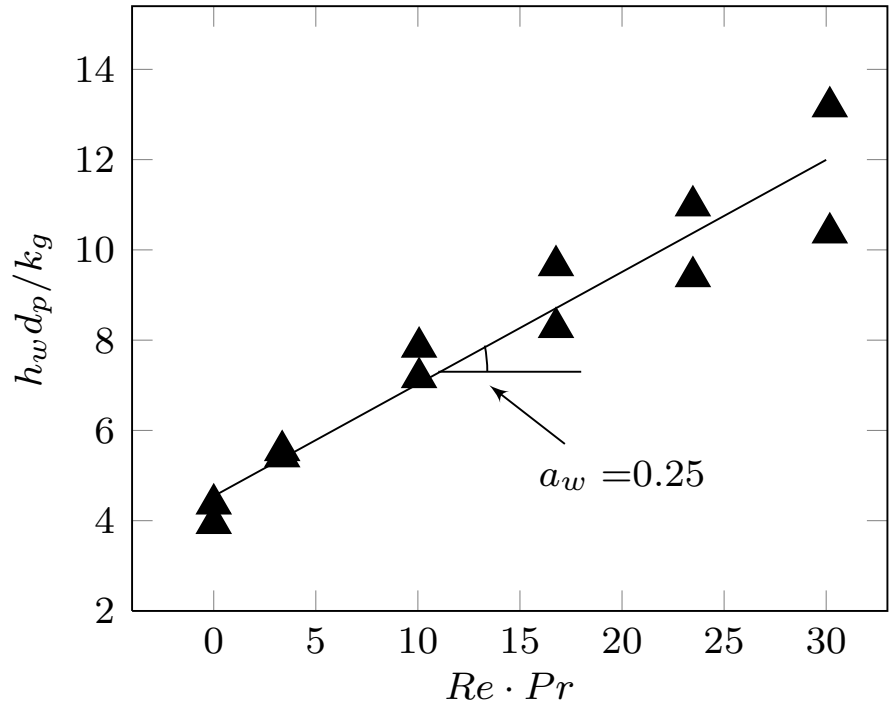

(b) PCM

Fig. 9. Evolution of the Nusselt number for (a) the sand and (b) the PCM in the fixed bed as a function of the product between the Reynolds and Prandtl numbers. Continuous lines are the results for the theoretical model with $a_w = 0.29$ for the sand and $a_w = 0.25$ for the PCM. $\varepsilon_w = 0.9$

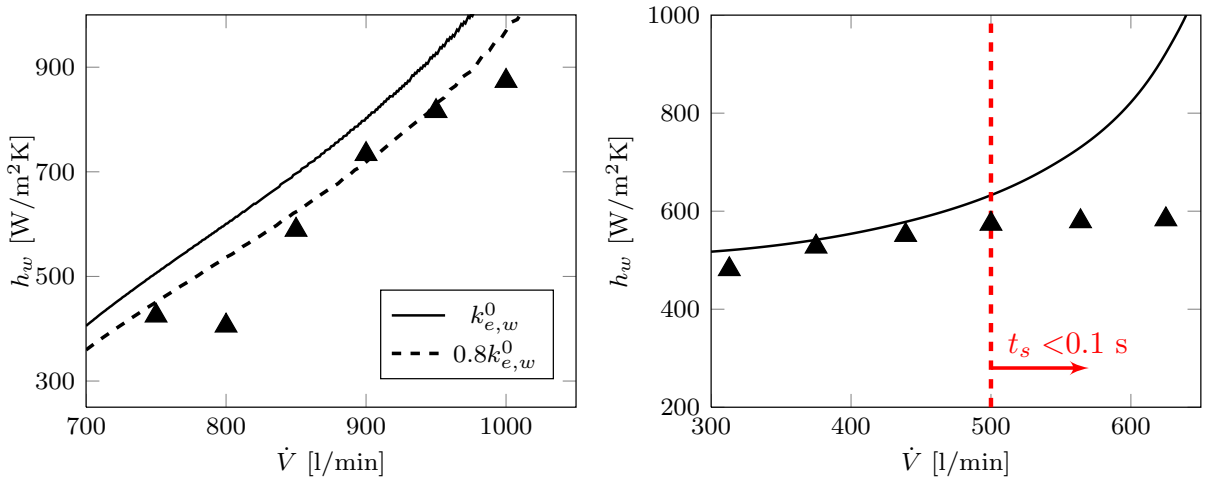

(a) Sand

(b) PCM

Fig. 10. Total heat transfer coefficient h_w calculated through the model (continuous line) and the experiments (isolated triangles) as a function of the flow for (a) the sand and (b) the PCM GR50. The dashed line Figure (a) represents the results of the model assuming a reduction of $20\,\%$ in the equivalent thermal conductivity at the wall.

List of Tables

Material	Bed	ρ [kg/m^3]	k [W/(m·K)]	$\overline{d}_p \pm \sigma_{d_p}$ [mm]	m [kg]
Sand	Fixed	2632.3	4.2	0.91 ± 0.13	13
	Fluidized	2632.3	4.2	0.76 ± 0.07	9
GR50	Fixed	1512.8	4.0	1.64 ± 0.20	8
	Fluidized	1550.5	4.0	0.54 ± 0.08	5

Table 1. Materials properties.